A TWO-COLOR PYROMETER FOR THE MEASUREMENT OF TEMPERATURE AND CONTAMINATION LEVEL IN A SPARK-HEATED HYPERVELOCITY WIND TUNNEL

by

Walter Vali

and

R. Stephen de Voto

Department of Aeronautics and Astronautics
Stanford University
Stanford, California

(The reproducible copy supplied by the authors was used in the reproduction of this report.)

August 1962

AF - AEDC
Arnold AFB Tenn

ABSTRACT

A description is given of exploratory measurements, by means of a two-color pyrometer, of the temperature and concentration of solid contaminants near the throat of a spark-heated hypervelocity wind tunnel. Because of its rapid response, the method is capable of providing a time-resolved history of the contamination during a run. Although some initial success can be reported, additional work remains to be done before the method can be made reliably quantitative and before the temperature of the flowing gas can be related to that of the contaminants.

CONTENTS

		Page
	ABSTRACT	iii
1.0	INTRODUCTION	1
2.0	TWO-COLOR PYROMETER	
	2.1 Theory	2
	2.2 Description of the Instrument	4
	2.3 Calibration	5
3.0	EXPERIMENTAL RESULTS	
	3.1 Typical Records	6
	3.2 Results and Discussion	7
	REFERENCES	9
	BIBLIOGRAPHY	10

ILLUSTRATIONS

Figure

1.	Pyrometer Optics	13
2.	Photomultiplier Circuit	14
3.	Calibration for Run 217. Ratio of Photomultiplier Currents vs. Temperature	15
4.	Pyrometer Traces	16
5.	Pyrometer Traces	17
6.	Integrated Light Output from Pyrometer. Run 217, without facing electrode. Horizontal Scale: 5 msec per large division	18
7.	Microscopic Picture of Dust. Scale: 1 inch = 21μ	19
8.	Calibration for Run 222. Ratio of Photomultiplier Current vs. Temperature	20
9.	Gas Temperature vs. Time for Various Area Ratios Near Throat - Run 222, without Facing Electrode	21
10.	Gas Temperature vs. Time for Various Area Ratios Near Throat - Run 217, without Facing Electrode	22
11.	Integrated Light Output vs. Weight of Contaminant Collected on Disc	23
12.	Comparison of Dust Collected on Disc in Test Section for Two Arc-Chamber Configurations	24
13.	Arc-Chamber Configurations	25

1.0 INTRODUCTION

A program of experimental and theoretical study of the performance of a spark-heated hypervelocity wind tunnel has been in progress at Stanford University since the summer of 1958. Reports by Karamcheti et al. (1961,1962), Vincenti (1961), and Emanuel and Vincenti (1962) describe some aspects of the work with regard to the state of the gas in the arc chamber, nozzle, and test section. This report describes the investigations being performed concerning the temperature and contamination level of the gas at a position 2.25 inches downstream of the throat of the wind-tunnel nozzle. If the chemical composition and/or vibrational energy freeze at some point in the flow, the static temperature will differ considerably from that for equilibrium flow. It would be valuable therefore to measure independently the static temperature of the gas and compare the value so obtained with that given by theoretical calculation.

Additional information obtained concerning the presence in the gas stream of fine contaminant dust is also of importance. These metallic or metal-oxide particles, formed in the arc chamber, are accelerated to a high velocity in the test section. The presence of the particles in the gas can affect aerodynamice measurements to a considerable degree. A method of monitoring and perhaps measuring the amount of contaminant present in the flow would therefore be desirable.

A variety of methods have been used for measuring the temperature of flames and hot gases and are well summarized by Broida (1955). In selecting a method to be used in the present case it must be remembered that the contaminant particles radiate with a continuous spectral distribution. This radiation from the contaminant immediately suggests the possibility of measuring the contaminant temperature and inferring the gas temperature. If the contaminant is in thermal equilibrium with the gas, then the gas and contaminant temperatures are identical. If we assume that this equilibrium does exist, then a method for measuring the contaminant temperature must now be found.

A commonly used method to measure directly the temperature of a gas is the line-reversal method. In this method, the radiation from a source gas of known temperature is compared with the radiation from the gas whose temperature is to be measured. The temperature of the source is adjusted until the intensity of radiation from the two gases is the same. While the adjustments of the source temperature are usually made manually, they could be done electronically, and so obtain the rapid response necessary for temperature measurement in the wind tunnel. Because of the difficulties inherent in the line-reversal method (the thermodynamic states of the source and the test gas have to be identical, i.e., same pressure, temperature, composition, etc.), the so-called two-color method was chosen instead for the present application.

---

* References are given at the end of the report. A bibliography of other sources of pertinent information is also appended.

The two-color method measures the intensity of radiation from the contaminant at two wave lengths in the continuous spectrum and deduces the temperature from the intensity ratio. If photomultiplier tubes are used as the intensity-measuring device, very rapid temperature fluctuations can be observed. Since the intensity of radiation must be measured in this method, it is also available as an indicator of the amount of contamination present in the gas. The following will describe the theory of this method and the results thus far obtained.

2.0 TWO-COLOR PYROMETER

2.1 THEORY

The electromagnetic radiation emitted by a solid or liquid body is in general distributed continuously over all wave lengths. The intensity I as a function of wave length λ at a given temperature T is described by Planck's distribution law

$$I = \frac{a}{\lambda^5(e^{b/\lambda T} - 1)} \quad , \tag{1}$$

where a and b are constants. Planck's law is strictly valid only for bodies that absorb all of the incident radiation ("black body"). Any physically realizable surface, however, is not black. The absorbtivity, as well as the emissivity, are in general functions of wave length and temperature. The intensity of radiation emitted by a surface is therefore rewritten as

$$I = \frac{\epsilon a}{\lambda^5(e^{b/\lambda T} - 1)} \quad , \tag{2}$$

where ϵ is the emissivity of the surface, which varies with temperature and wave length. For moderate temperatures (a few thousand degrees K) and radiation observed in or near the visible range $\lambda T < b$, we can approximate equation (2) by

$$I = \epsilon a \lambda^{-5} e^{-b/\lambda T} \quad . \tag{3}$$

By measuring the intensity of a light in the narrow wave-length bands around λ_1 and λ_2, we can express the ratio of the intensities as a function of temperature from equation (3) as

$$\frac{I_1}{I_2} = \left(\frac{\lambda_2}{\lambda_1}\right)^5 \frac{\epsilon_1}{\epsilon_2} e^{(b/T)(1/\lambda_2 - 1/\lambda_1)} \quad .$$

From this we find

$$T = b\left(\frac{1}{\lambda_2} - \frac{1}{\lambda_1}\right) \ln\left[\left\{\left(\frac{\epsilon_2}{\epsilon_1}\right)\left(\frac{\lambda_1}{\lambda_2}\right)^5\left(\frac{I_1}{I_2}\right)\right\}\right]^{-1} \quad . \qquad (4)$$

In equation (4) the single constant b has the value

$$b = \frac{hc}{k} = 1.42 \text{ cm deg K} \quad .$$

Thus, by measuring the intensity of radiation in two narrow wave-length bands, the temperature can be calculated provided the emissivities are known.

In the present case the two wave-length bands have actually been taken a few thousand angstroms wide. The choice of wide bands has two important advantages: first, it increases the total intensity of radiation, and second, it simplifies the equipment considerably. As a result, however, the simple equation (4) can no longer be used to find the temperature. The total emission in a wide band is

$$I_1 = a\int_{\lambda_1}^{\lambda_1 + \Delta\lambda_1} \epsilon(T,\lambda)\lambda^{-5} e^{-(b/\lambda T)} d\lambda \quad , \qquad (5)$$

where $\Delta\lambda_1$ is the band width. Since the photocurrent is the quantity actually recorded, the phototube output is given by

$$i_1 = a\int_{\lambda_1}^{\lambda_1 + \Delta\lambda_1} \epsilon(T,\lambda)\lambda^{-5}\eta(\lambda) e^{-(b/\lambda T)} d\lambda \quad , \qquad (6)$$

where $\eta(\lambda)$ is the quantum efficiency of the photosensitive surface of the photomultiplier tube. The ratio of the photocurrents of the two wave-length bands is therefore

$$\frac{i_1}{i_2} = \frac{\int_{\lambda_1}^{\lambda_1+\Delta\lambda_1} \epsilon(\lambda,T)\eta_1(\lambda)\lambda^{-5}\, e^{-(b/\lambda T)}\, d\lambda}{\int_{\lambda_2}^{\lambda_2+\Delta\lambda_2} \epsilon(\lambda,T)\eta_2(\lambda)\lambda^{-5}\, e^{-(b/\lambda T)}\, d\lambda} \quad . \qquad (7)$$

The ratio of the photocurrents is thus a function of temperature. If the emissivities and quantum efficiencies are known, the temperature can be calculated. The numerical integrations involved in equation (7) are avoided, however, through the calibration of the instrument by means of static high-temperature sources. A detailed description of the method of calibration will be given later.

2.2 DESCRIPTION OF INSTRUMENT

As shown in Fig. 1, the pyrometer consists essentially of two photomultiplier tubes. No filters or prisms are used to make the two wave-length bands narrow. Instead, the tubes have been chosen so that one (Dumont 6292) has a sensitivity range of 3500 Å to 5500 Å , while the other (Dumont 6911) is sensitive from 6000 Å to 9000 Å . The phototubes themselves thus act as broad-band filters. Light entering the pyrometer through the window is collimated by a lens of 3-inch focal length. An adjustable diaphragm is used to obtain a suitable lens opening during calibration. This is necessary since the intensity of radiation increases as the temperature of the source increases ($\sim T^4$). The lens opening therefore has to be decreased in order to maintain the amplifier gain at the same setting as used during the run of the tunnel. After passing through the diaphragm, the light beam is split into two parts by a half-silvered mirror. The two beams thus formed then fall simultaneously on the two phototubes.

The electronic circuit for the photomultipliers is shown in Fig. 2. It was decided to use negative high voltage on the photo cathode and thus obtain an output close to the ground potential. This necessitated the use of two cathode followers for the following reason: The output from a cathode follower without a signal voltage on the grid is a few volts. The signal, being negative, decreases this zero output voltage. In order to observe these small changes in the output potential, it is necessary to balance out the zero voltage. The simplest way to accomplish this is through the use of a second cathode follower whose output can be varied manually until its output balances the zero output of the first follower. The power supply used for the phototube is a Model 412A from the John Fluke Co.

2.3 CALIBRATION

Equation (7) contains the empirical function $\eta(\lambda)$, the efficiency of the photosensitive surface. Since this varies considerably from one phototube to another and also with time, it was decided to calibrate the phototubes statically. To accomplish this, a heated platinum strip is placed behind the small window in the nozzle wall. The light emitted by this strip passes through the window and the lens and is reflected by the mirrors - the same light path as used during the actual run. This procedure eliminates the necessity of corrections due to the somewhat selective transmissivities and reflectivities of the optical components of the pyrometer.

The voltage on the photomultiplier tubes for most runs is between 800 and 1000 volts. The output of both phototubes is adjusted to zero with the diaphragm closed. After opening the diaphragm, the outputs are then recorded on a dual-beam oscilloscope. At the same time, the temperature of the platinum strip is measured by means of a Leeds and Northrup hot-wire pyrometer. This procedure is repeated at intervals of about 50° from 1300° to 1700°K. A typical calibration curve is shown in Fig. 3. The absolute value of the ratio as recorded on an oscilloscope can be adjusted arbitrarily by changing the amplification of the balanced input amplifiers (part of the oscilloscope).

The foregoing calibration was also repeated with an oxidized nichrome ribbon whose emissivity is closer to unity than is that of the platinum. The difference in calibration curves is noticeable. It is probable that the emissivity of the dust in the flow is somewhere between those of platinum and nichrome.

An additional calibration is performed after the wind tunnel is fired. The calibration curve changes considerably as shown in Fig. 3. This is due to deposition of dust on the inside surface of the window. As seen from Fig. 3, the transmissivity of the red light decreases less than does that of the blue. This is to be expected from the theory of absorption and scattering of light.

Calibration is routinely performed immediately before and after each run. The calibration curves used to compute the temperature are generally the "before-run" curves, since it seems plausible that most of the dust is deposited on the window during the final part of the run. Before calibration, the power supplies and filaments are allowed to warm up for a minimum of 30 minutes.

3.0 EXPERIMENTAL RESULTS

3.1 TYPICAL RECORDS

All temperature measurements were made at a position 2.25-inches downstream of the throat of the nozzle. At this position the theoretical equilibrium gas temperature is around 1000°K. This is somewhat lower than the minimum temperature used for the calibration. The actual measurements, however, put the observed contaminant temperature well within the range of the calibration.

The pyrometer is used during nearly every run of the tunnel. Because of the large variation of the intensity of the emitted light, the data from only about half the runs are usable. The output of the phototubes is displayed on a dual-beam oscilloscope, which is triggered by a signal from a coil placed near one of the capacitors of the main wind-tunnel bank. Sweep speeds are generally between 1 and 5 millisec per cm. The traces are recorded on Polaroid 3000-speed film. After each run a zero-output trace is recorded on the film.

As mentioned, the intensity variation from shot to shot is considerable. This makes it difficult to set the preamplifier gain correctly. If the gain is too low, then one or both of the trace deflections are too small to be measured accurately. If it is too high, one or both of the traces are deflected off scale. (This difficulty will be circumvented in the future by the use of a simple analogue computer whose output is the ratio of the two photomultiplier outputs.)

Fig. 4a shows the record of Run 222. It is typical of the usable records. The high contamination level started about 1.5 millisec after the start of the run. Fig. 4b shows a similar run on an expanded time scale showing clearly a relatively clean flow for the first 2 millisec. Both of these runs were made with the arc-chamber configuration designated "without facing electrode" (see Fig. 13). Figs. 5a and 5b show two typical shots with the facing electrode in the arc-chamber. A noticeable feature is the relatively long period of clean flow (approximately 10 millisec) compared with the previous results without the electrode. Once arrived, the contamination continues at a relatively high level for a longer period of time.

Some measurements were also made of the total amount of contaminant dust as observed by one phototube (Dumont 6911). The integrated light output is shown on one trace of Fig. 6. The other trace is the direct output from the same phototube.

An attempt was made to measure the size of the dust particles with an optical microscope. As seen from Fig. 7, the size of single particles (not agglomerates) is less than 1 micron in diameter, which makes the use of an optical microscope questionable. An electron microscope would be needed to give reliable particle-size measurements.

3.2 RESULTS AND DISCUSSION

Fig. 4a gives the recorded photomultiplier outputs as previously described. The corresponding calibration before the run is shown in Fig. 8. By taking the ratio of the deflection of the upper trace in Fig. 4a to that of the lower trace at the same instant, the temperature can be obtained from the calibration curve. The temperature as a function of time is plotted in Fig. 9. The same procedure was repeated for Run 217, the results for which are shown in Fig. 10. These plots also include the equilibrium-flow temperature for various area ratios as calculated theoretically on the basis of the measured arc-chamber conditions. At the pyrometer station the geometric area ratio is 15. Since the boundary-layer thickness is at present unknown, the effective area ratio cannot be estimated accurately.

It is evident that the measured contaminant temperatures are considerably higher than the calculated gas temperatures. In the light, however, of the recent spark-disturbance measurements of the velocity of flow in the test section (Karamcheti, Vali, and Kyser, 1962), it appears that the calculated temperatures should be increased by up to 60 per cent. This would bring the calculated temperatures fairly close to the observed temperature.

As seen from Figs. 4 and 5, the light intensities vary rapidly with time. Variations in light intensity will occur only when either the radiating-surface area changes or the temperature changes. Since the temperature variations during the run are small (cf. Figs. 9 and 10), the main fluctuations appear to be caused by the change of radiating-surface area at the pyrometer position. It follows from this that the dust cloud opposite the pyrometer window is optically thin and that the dust density must vary considerably during a run.

Some preliminary measurements were made to compare the time-integrated output from a photomultiplier with the weight of dust collected on a disc placed on the center line of the test section. The results are shown in Fig. 11. The relatively large scattering of the points can probably be attributed to a nonuniform distribution of the dust in the gas, both radially and (especially) in time. Whereas the time integration of the photomultiplier output includes practically all of the flow out of the arc chamber, the disc probably collects dust only for the duration of the supersonic flow in the test section. Therefore, in the shots where the large amounts of dust come late in the flow from the arc chamber, the collector-disc pickup is considerably decreased. There is also some question concerning the minimum size of dust particle that the disc can collect. Particles of a very small diameter tend to follow the flow and thus never hit the collector disc. These very small particles contribute relatively more strongly to the radiation than to the collected weight, since, for the same specific gravity of dust, the radiation is proportional to the radius squared, while the weight is proportional to the radius cubed.

As shown in Fig. 12, the amount of contaminant collected by the disc depends strongly on the arc-chamber configuration. It may be that, in the absence of the facing electrode, the relatively clean, central core of the arc-chamber gas flows out first, giving the dust in the chamber more time to collect on the cool walls. With the facing electrode present, however, the gas may flow out peripherally, thus carrying with it somewhat more dust. The fact that the supports for the facing electrode are difficult to clean between runs may also contribute to the situation. (The data of Figs. 11 and 12 were taken over a considerable period of time and are not necessarily representative of current best practice; cf. van der Bliek (1962) and Bianchetta and Sivier (1962).)

With regard to the question of thermal equilibrium between the dust and gas, no definite conclusions can be drawn at present. The decrease of the temperature of the dust as it flows down the nozzle proceeds through two independent processes: (1) radiation, and (2) conduction of heat to the surrounding gas. The radiation losses are easily evaluated for small, spherical, highly conducting bodies. It can be shown that the time required for a dust particle to drop from temperature T_2 to temperature T_1 is

$$t = \frac{r\rho c}{9\epsilon\sigma}\left(\frac{1}{T_1^3} - \frac{1}{T_2^3}\right) ,$$

where r is the radius of the particle, ρ its density, c its specific heat, ϵ its emissivity, and σ is the Stefan-Boltzmann constant. Applied to 0.1-micron iron spheres, this gives about 60 microseconds for the time required for a temperature drop from 4000°K to 2000°K. This is considerably longer than the time required for the gas to travel from the throat to the pyrometer window (~ 25 microsec). The rate of heat loss through conduction to the gas has not yet been calculated. The results presented by Hoglund (1962) indicate, however, that the temperature of particles of diameter less than a micron will follow the gas temperature fairly closely.

There are a number of factors that need to be investigated further before completely reliable temperature measurements can be made. Some of these are:

(1) Nonuniformity of the gas temperature at the pyrometer station,

(2) Rate of heat loss from the dust through conduction,

(3) Scattering of radiation coming from the arc chamber (opacity of the dust between the throat and the pyrometer station),

(4) Emissivity of the dust,

(5) Effect of particle size on the distribution of radiated energy.

REFERENCES

Bianchetta, J. F., and Sivier, K. R., 1962, "Operating Experience with the M.A.C. Hypervelocity Impulse Tunnel", in 'Advances in Hypervelocity Techniques', ed. by A. M. Krill, Plenum Press.

Broida, H. P., 1955, "Experimental Temperature Measurements in Flames and Hot Gases", in 'Temperature, Its Measurement and Control in Science and Industry', Reinhold.

Emanuel, G., and Vincenti, W. G., 1962, "Method of Calculation of the One-Dimensional Nonequilibrium Flow of a General Gas Mixture through a Hypersonic Nozzle", AEDC-TDR-62-131.

Hoglund, R. F., 1962, "Recent Advances in Gas-Particle Nozzle Flows", ARS Journal, 32, p. 662.

Karamcheti, K., Vali, W., and Vincenti, W. G., 1961, "Initial Experience with the Stanford Spark-Heated Hypersonic Wind Tunnel", Stanford University Department of Aero. Engr., SUDAER No. 100.

Karamcheti, K., Vali, W., and Kyser, J. B., 1962, "Optical Techniques for the Measurement of Velocity, Density, Temperature, and Contamination Level in a Spark-Heated Hypervelocity Wind Tunnel", Paper at the Second National Symposium on Hypervelocity Techniques, Denver, Colorado, March 20-21, 1962.

van der Bliek, J. A., 1962, "Further Development of Capacitance- and Inductance-Driven Hotshot Tunnels", in 'Advances in Hypervelocity Techniques', ed. by A. M. Krill, Plenum Press.

Vincenti, W. G., 1961, "Calculations of the One-Dimensional Nonequilibrium Flow of Air through a Hypersonic Nozzle - Interim Report", AEDC-TN-61-65.

BIBLIOGRAPHY

Anon., 1959, Dumont Photomultiplier Tube Handbook, Dumont Laboratories.

Crandall, S. H., 1956, "Engineering Analysis", McGraw-Hill.

DeVos, J. C., 1954, "The Emissivity of Tungsten Ribbon", Physica, 20, p.690.

Eckert, E. R. G., and Drake, R. M., 1959, "Heat and Mass Transfer", McGraw-Hill.

Fishendon, M., and Saunders, O. A., 1948, "Waste Heat Recovery from Industrial Furnaces", Chapman & Hall.

Grabau, M., Humphrey, R. L., and Little, Wanda J., 1961, "Determination of Test-Section, After-Shock, and Stagnation Conditions in Hotshot Tunnels using Real Nitrogen at Temperatures from 3000 to 4000°K", Arnold Engineering Development Center, AEDC-TN-61-82.

Heidman, M. F., and Priem, R. J., 1953, "Application of the Electro-Optical Two-Color Pyrometer to Measurement of Flame Temperature for Liquid Oxygen-Hydrocarbon Propellant Combination", Nat. Adv. Com. for Aero., NACA TN 3033.

Hottel, H. C., and Broughton, F. P., 1932, "Determination of True Temperature and Total Radiation from Luminous Gas Flames", Ind. and Eng. Chem., Anal., Ed. 4, No.1, p.166.

Hulburt, E. O., 1915, "The Reflecting Power of Metals in the Ultra-Violet Region of the Spectrum", Astrophysical Journal, 42, p.203.

Kohl, W. H., 1960, "Materials and Techniques for Electron Tubes", Reinhold.

McAdams, W. H., 1954, "Heat Transmission", McGraw-Hill.

McCauley, G. V., 1913, "The Energy Spectra of Platinum, Palladium, and Tantalum", Astrophysical Journal, 37, p.164.

Mie, G., 1908, "Beiträge zur Optik Trüber Medien, Speziell Kolloidaler Metallösungen", Annalen der Physik, Leipzig, 25, p.377.

Pivovonsky, M., and Nagel, M. R., 1961, "Tables of Black Body Radiation Functions", Macmillan.

Uyehara, O. A., Myers, P. S., Watson, K. M., and Wilson, L. A., 1946, "Flame Temperature Measurements in Internal Combustion Engines", Trans. A.S.M.E., 68, No.1, p.17.

BIBLIOGRAPHY (Concl'd)

Wolfhard, H. G., and Parker, W. G., 1948, "Emissivity of Small Particles in Flames", Nature, 162, p.259.

Wolfhard, H. G., and Parker, W. G., 1949, "Temperature Measurements of Flames Containing Incandescent Particles", Proceedings Physical Society, (London), B.62, p.523.

Worthing, A. G., 1926, "Special Emissivities of Tantalum, Nickel and Gold as Functions of Temperature and the Melting Point of Tantalum, Physical Review, 28, p.174.

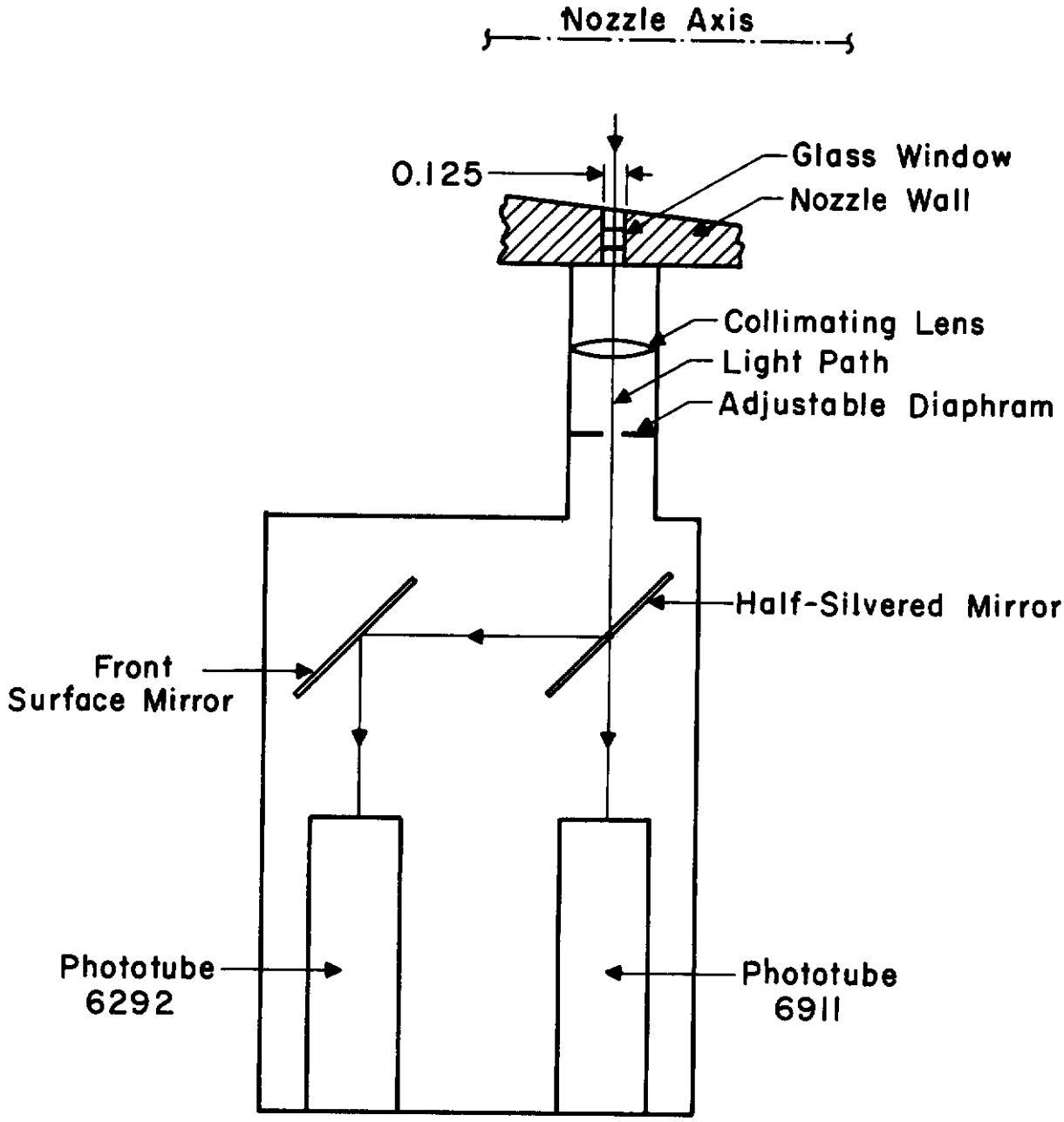

Fig. 1 Pyrometer Optics

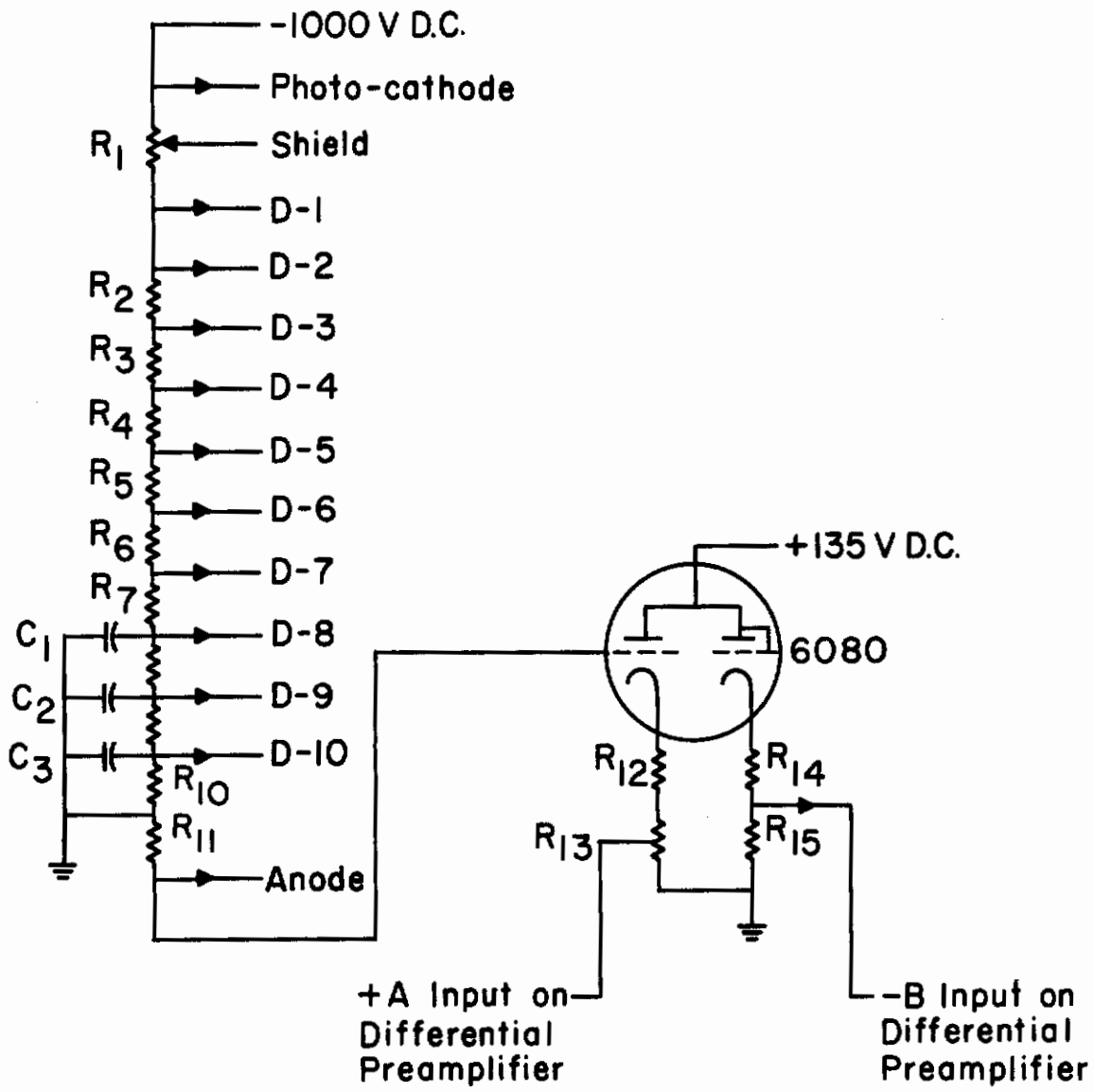

R_1 : 50 KΩ
R_2-R_{10} : 27 KΩ
R_{11} : 1 MΩ
R_{12} , R_{15} : 100 Ω
R_{13} : 500 Ω
R_{14} : 470 Ω
C_1 : 0.05 μf., 600 V
C_2 : 0.05 μf., 400 V
C_3 : 0.10 μf., 400 V

Fig. 2 Photomultiplier Circuit

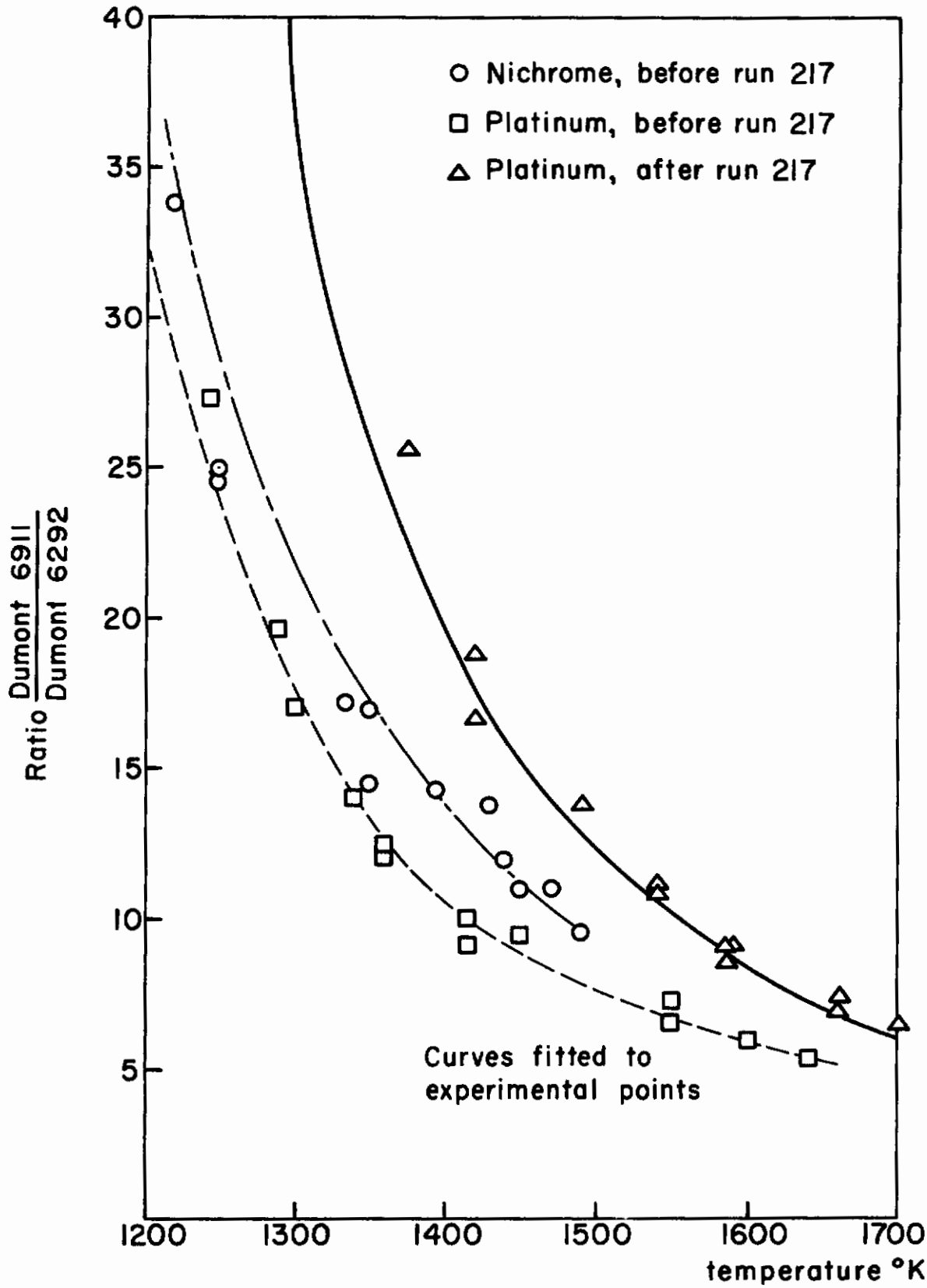

Fig. 3 Calibration for Run 217. Ratio of Photomultiplier Currents vs. Temperature

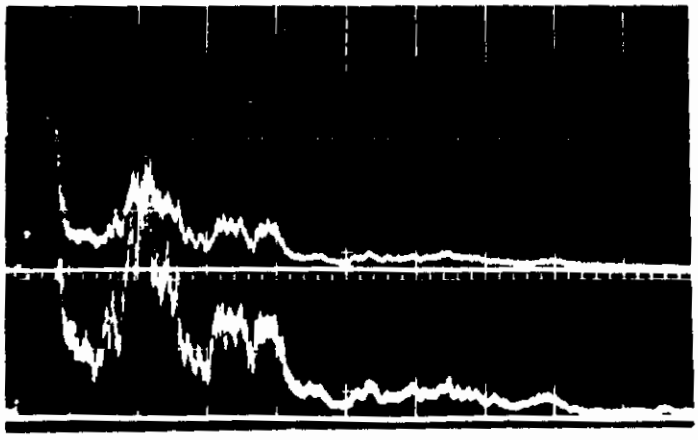

4a. Run 222
Without facing electrode
Horizontal Scale: 5 msec per large division

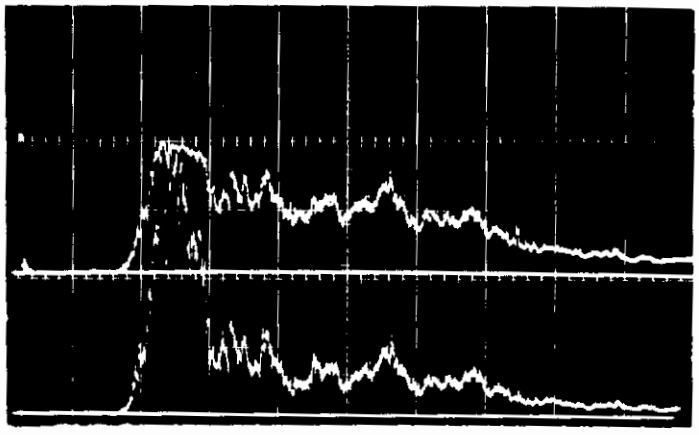

4b. run 225
Without facing electrode
Horizontal Scale: 1 msec per large division

Fig. 4 Pyrometer Traces

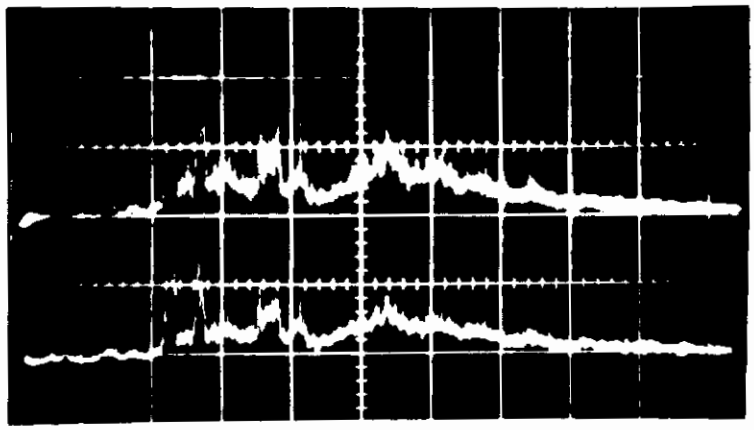

5a. Run 175
with facing electrode
Horizontal Scale: 5 msec per
large division

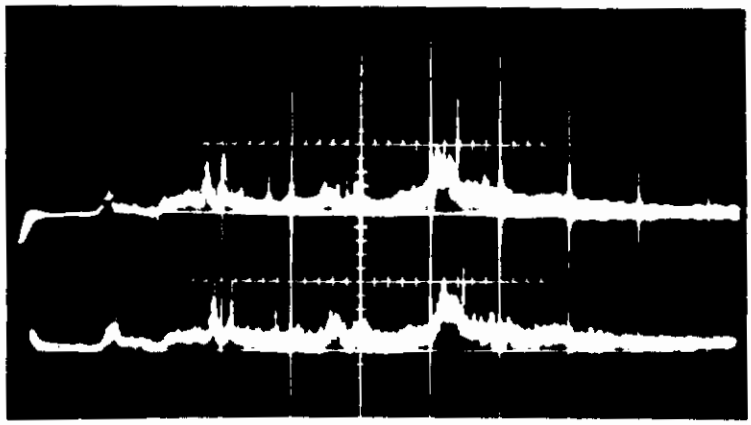

5b. Run 176
with facing electrode
Horizontal Scale: 5 msec per
large division

Fig. 5 Pyrometer Traces

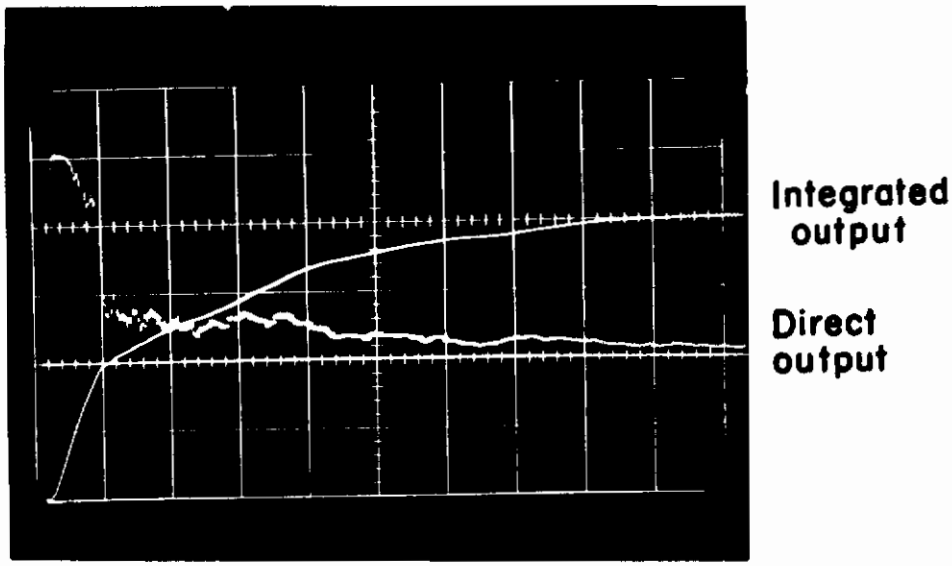

Fig. 6 Integrated Light Output from Pyrometer.
Run 217, without facing electrode.
Horizontal Scale: 5 msec per large division

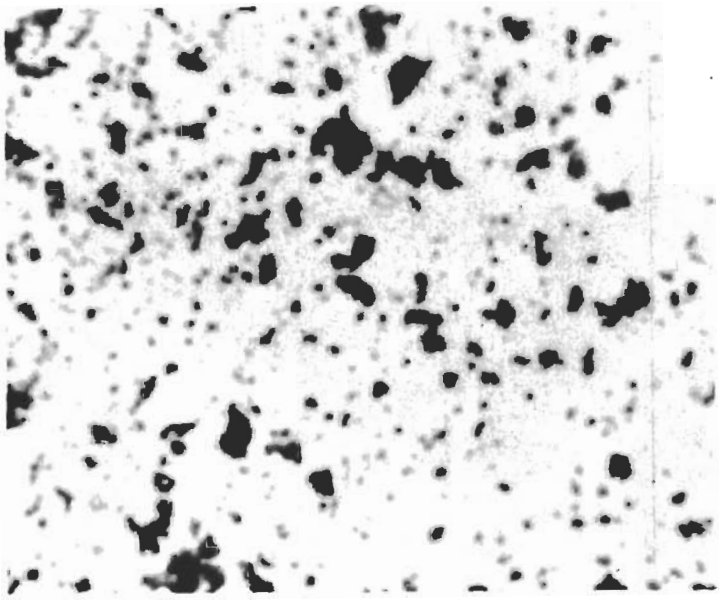

Fig. 7 Microscopic Picture of Dust.
Scale: 1 inch = 21 μ

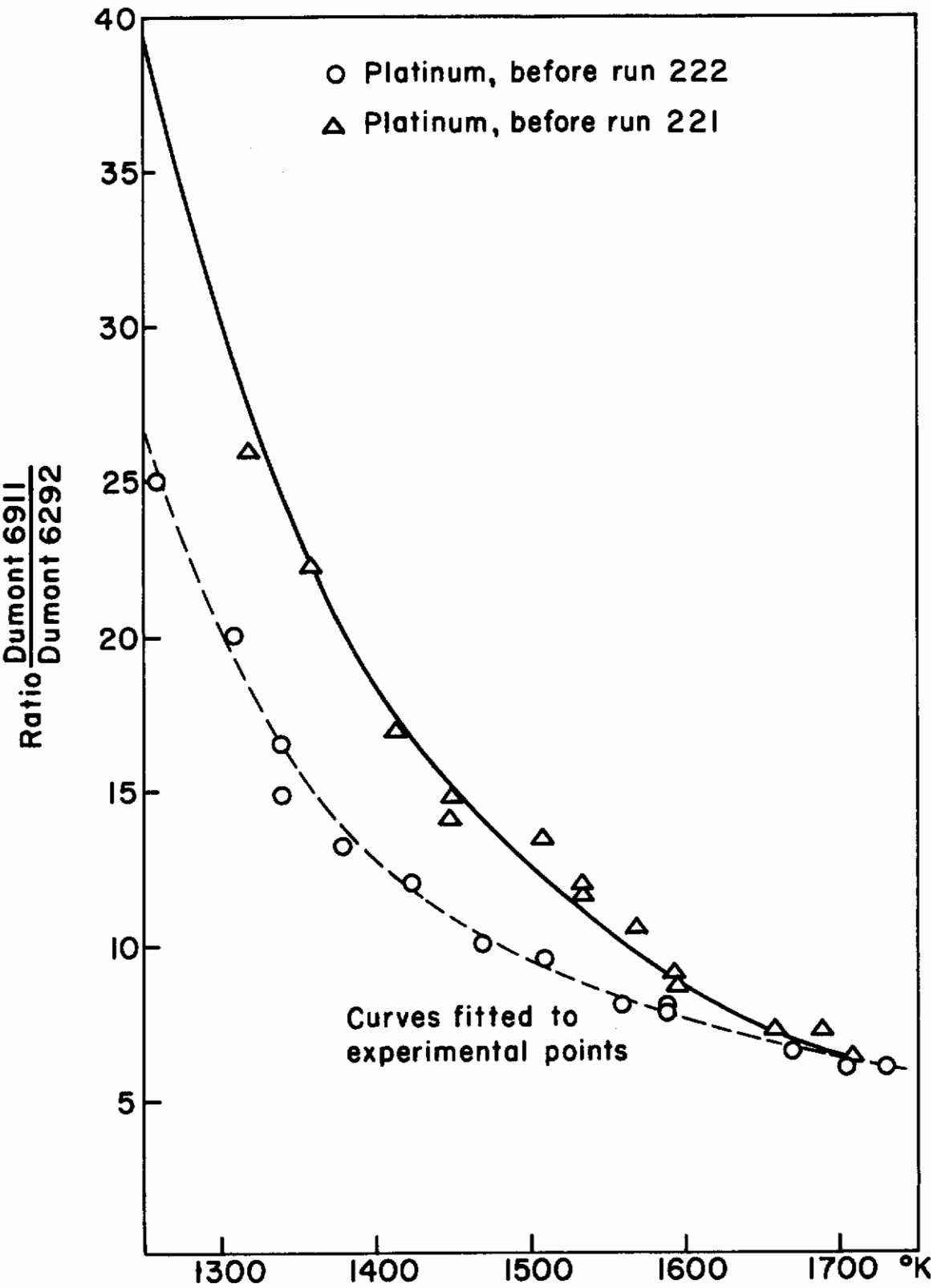

Fig. 8 Calibration for Run 222. Ratio of Photomultiplier Currents vs. Temperature

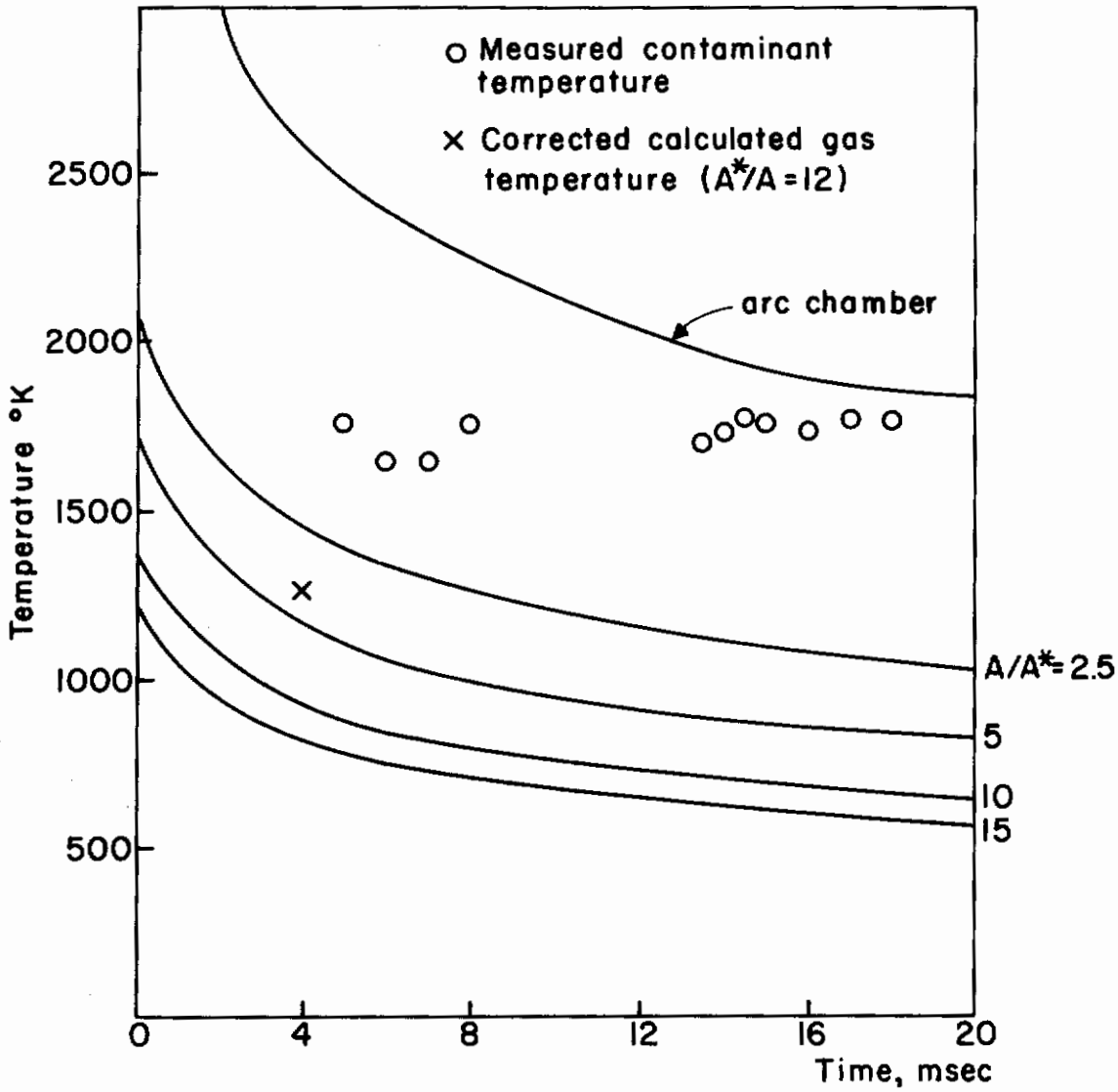

Fig. 9 Gas Temperature vs. Time for Various Area Ratios Near Throat - Run 222, without Facing Electrode

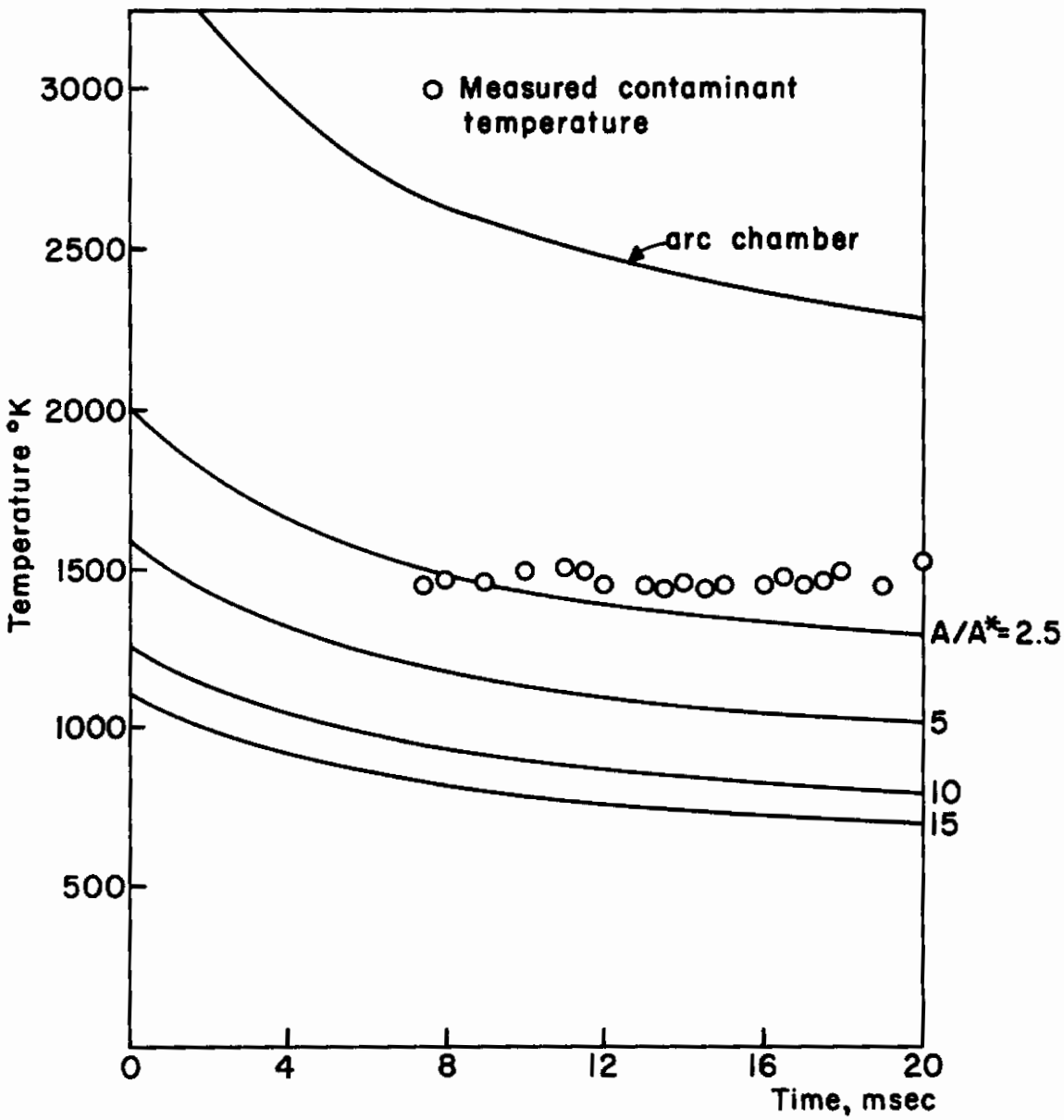

Fig. 10 Gas Temperature vs. Time for Various Area Ratios Near Throat - Run 217, without Facing Electrode

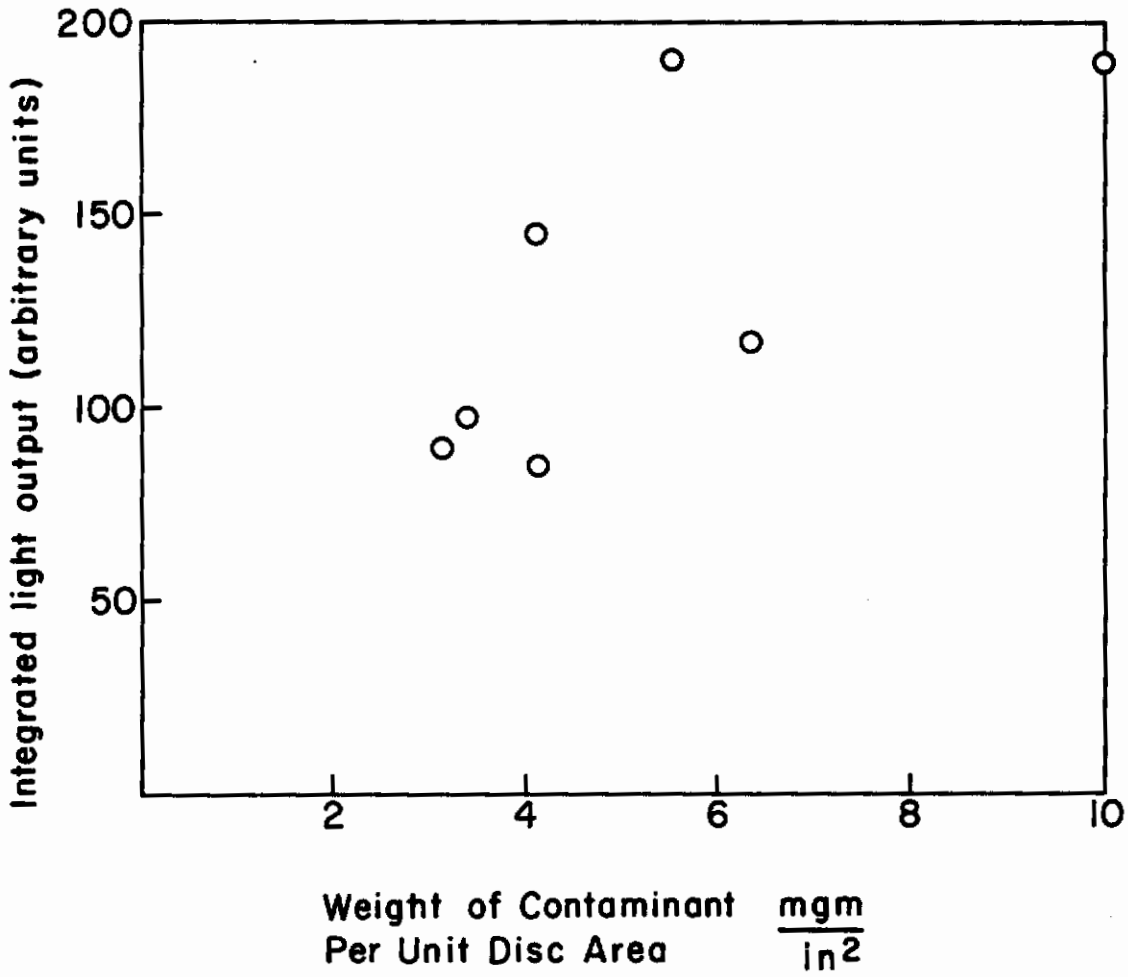

Fig. 11 Integrated Light Output vs. Weight of Contaminant Collected on Disc

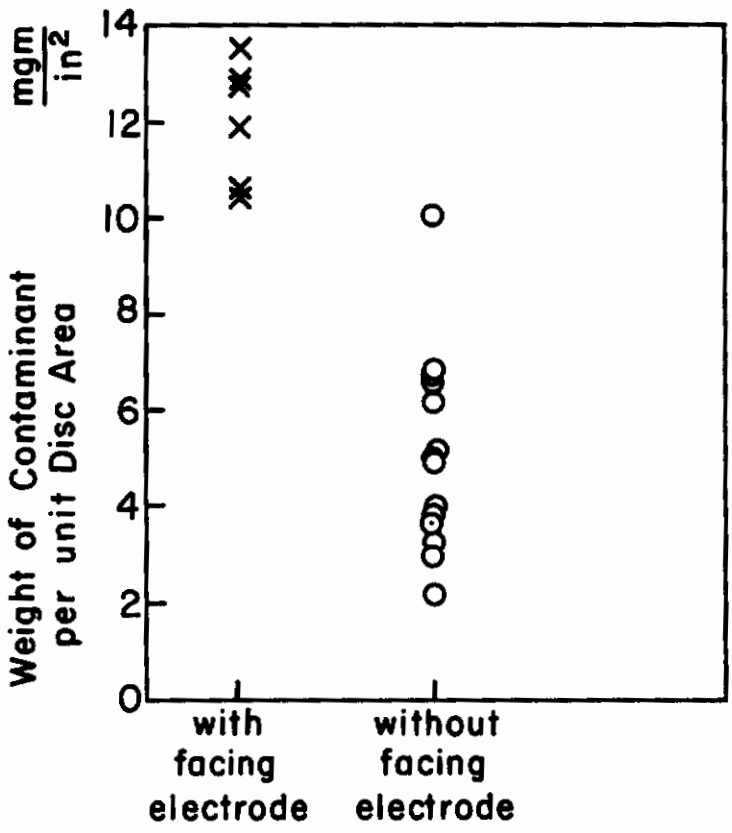

Fig. 12 Comparison of Dust Collected on Disc in Test Section for Two Arc-Chamber Configurations

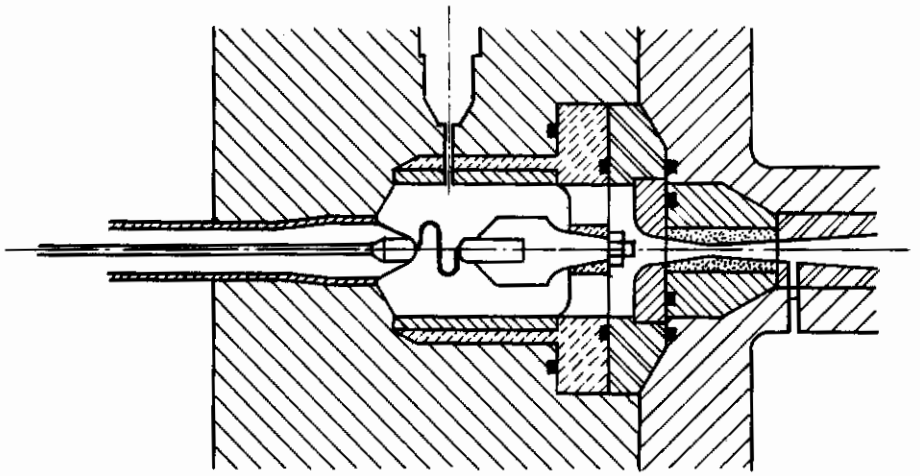

with facing electrode

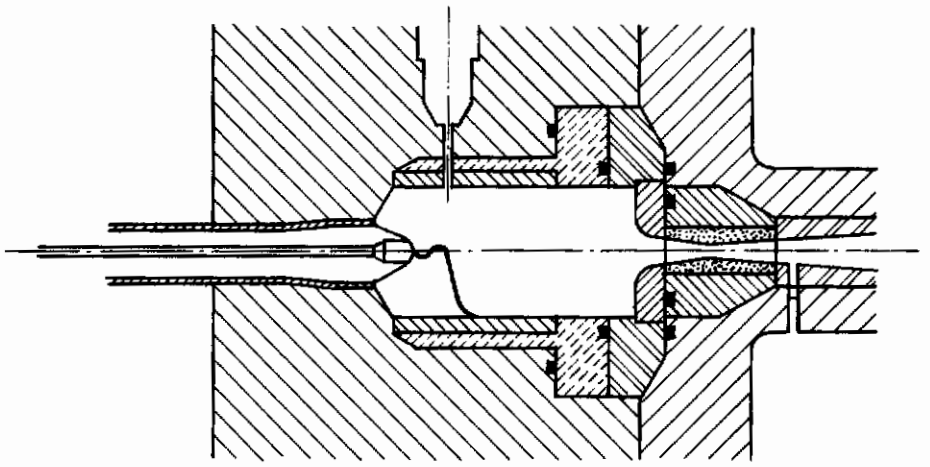

without facing electrode

Fig. 13 Arc-Chamber Configurations